SPLITTING OF INVISCID FLUXES FOR REAL GASES

88-3526-CP

Meng-Sing Liou
NASA Lewis Research Center, Cleveland, Ohio

Bram van Leer
The University of Michigan, Ann Arbor, Michigan and
Institute for Computational Mechanics in Propulsion (ICOMP),
NASA Lewis Research Center, Cleveland, Ohio

and

Jian-Shun Shuen
Sverdrup Technology, Inc., Middleburg Heights, Ohio and
NASA Lewis Research Center, Cleveland, Ohio

ABSTRACT

Flux-vector and flux-difference splittings for the inviscid terms of the compressible flow equations are derived under the assumption of a general equation of state for a real gas in equilibrium. No unnecessary assumptions, approximations or auxiliary quantities are introduced. The formulas derived include several particular cases known for ideal gases and readily apply to curvilinear coordinates. Applications of the formulas in a TVD algorithm to one-dimensional shock-tube and nozzle problems show their quality and robustness.

1. INTRODUCTION

Several split-flux formulas are known for upwind differencing of the inviscid terms in CFD codes for ideal gases. The generic formula is due to Gudonov [1] and is based on the exact solution of Riemann's initial-value problem, representing the interaction of two fluid parcels by finite-amplitude waves.

Numerical efficiency justifies the introduction of approximations to the Riemann solution, which leads to various simplifications of the flux formula, accompanied by considerable savings in computational expenses. The most popular "approximate Riemann solvers" are the flux-vector splittings by Steger and Warming [2] and by Van Leer [3] and the flux-difference splittings by Roe [4] and by Osher [5]; see e.g., the review by Harten, Lax and Van Leer [6].

With the current interest in high-temperature flows, real-gas effects* must be included, requiring appropriate modifications of all of the above split-flux formulas. Colella and Glaz [7] extended the numerical procedure for obtaining the exact Riemann solution to the real-gas case. Grossman and Walters [8], as well as Vinokur and Liu [9] extended the formulas of Steger and Warming, Van Leer and Roe, while Glaister [10] presented an extension of the Roe splitting.

The present derivation of split-flux formulas has the following features:(1) it includes several particular formulas derived elsewhere for ideal gases, (2) it avoids unnecessary assumptions or approximations, (3) it avoids unnecessary auxiliary quantities, and (4) it readily extends to curvilinear coordinates.

In the next section we briefly discuss the equation of state (EOS) for the real gas and some related thermodynamics quantities. The detailed derivation of split-flux formulas is given in Section 3. Application of this construction in a TVD algorithm [11] is demonstrated for one-dimensional shock tube and nozzle problems.

2. EQUATION OF STATE

We begin by assuming that the real gas is described by the general equation of state,

$$p = p(\rho, e, Y_i), \qquad i = 1, 2, 3... \tag{2.1}$$

where p, ρ, e, Y_i are, respectively, the pressure, density, and specific internal energy of the gas and the mass fraction of the i-th species in the gas. In this paper, we will restrict ourselves to the gas in chemical equilibrium, i.e.,

$$p = p(\rho, e), \tag{2.2}$$

so that derivatives with respect to Y_i disappear, simplifying the algebra. Yet, the concepts and algebraic steps needed to describe a non-equilibrium gas are very nearly the same as for the equilibrium gas. In fact, some of the special care in formulating the EOS of an equilibrium gas can be relaxed when including nonequilibrium (finite-rate reaction) effects, because the overall numerical procedure becomes more straightforward. The computational effort, of course, is increased enormously.

For an ideal gas, (2.2) reduces to $p = (\gamma - 1)\rho e$, where γ is the ratio of enthalpy h to internal energy e, and is a constant.

The speed of sound is

$$a^2 = p_\rho + p p_e / \rho^2. \tag{2.3}$$

* In this paper the definition of "real gas" is broader than that conventionally used in thermodynamics, by referring to any gas that is not both thermally and calorically perfect.

Here and in this paper, p_ρ and p_e denote the partial derivatives of p with respect to ρ and e while holding other variables fixed.

Several authors [7-9] have advocated the use of an equivalent γ for real gases. As in the ideal gas, we define

$$\gamma = h/e, \qquad h = \text{specific enthalpy}; \tag{2.4}$$

combining this with the definition, $h = e + p/\rho$, gives

$$p = (\gamma - 1)\rho e. \tag{2.5a}$$

This is identical in form to the EOS of the ideal gas, but now

$$\gamma = \gamma(\rho, e). \tag{2.5b}$$

The speed of sound expressed in terms of γ now has the form

$$a^2 = \gamma p/\rho + e\left[(\gamma - 1)e\gamma_e + \rho\gamma_\rho\right], \tag{2.6a}$$

where $\gamma_e = \partial\gamma/\partial e$ and $\gamma_\rho = \partial\gamma/\partial\rho$. Since for an ideal gas (2.6a) reduces to $a^2 = \gamma p/\rho$, this motivates the introduction of an auxiliary variable Γ such that

$$a^2 = \Gamma p/\rho = \Gamma(\gamma - 1)e, \tag{2.6b}$$

where $\Gamma = \Gamma(\rho, e)$.

We caution that the appearance of these different "equivalent γ's" may at times add more confusion than insight.

From thermodynamic principles, it is possible to calculate any thermodynamic variable for each pair of state quantities (ρ, e). In practice, a table or a least-square fitted surface is generated a priori for reasons of computational efficiency. We adopt the latter approach because interpolation is avoided, resulting in greater efficiency. However, care must be taken to ensure, while fitting, not only that the error is kept whithin reasonable bounds but also that no numerical oscillations are introduced.

3. CONSTRUCTION OF SPLIT FLUXES

To illustrate how the three split-flux formulas are constructed, we first consider the 1D Euler equations,

$$\frac{\partial \mathbf{U}}{\partial t} + \frac{\partial \mathbf{F}(\mathbf{U})}{\partial x} = 0 \tag{3.1}$$

where $E = e + u^2/2$, $\mathbf{F}^t = \left[\rho u, \rho u^2 + p, (\rho E + p)u\right]$, and $\mathbf{U}^t = [\rho, \rho u, \rho E]$.

As indicated previously, the EOS now is expressed in terms of all variables $\mathbf{U}$, viz. as $p = p(\rho(\mathbf{U}), e(\mathbf{U}))$. Thus the Jacobian matrix is readily derived,

$$\mathbf{A} = \frac{\partial \mathbf{F}}{\partial \mathbf{U}} = \mathbf{A}_e + \mathbf{A}_\rho, \tag{3.2a}$$

where

$$\mathbf{A}_e = \begin{pmatrix} 0 & 1 & 0 \\ -u^2(2 - p_e/\rho)/2 + (p - p_e e)/\rho & u(2 - p_e/\rho) & p_e/\rho \\ u[-H + u^2 p_e/2\rho + (p - p_e e)/\rho] & H - u^2 p_e/\rho & u(1 + p_e/\rho) \end{pmatrix}$$

contains the derivative p_e, and the matrix containing p_ρ is

$$\mathbf{A}_\rho = \begin{pmatrix} 0 & 0 & 0 \\ p_\rho - p/\rho & 0 & 0 \\ u(p_\rho - p/\rho) & 0 & 0 \end{pmatrix}, \tag{3.2c}$$

where $H = E + p/\rho$ is the specific total enthalpy.

The eigenvalues of these matrices are respectively: $\lambda(\mathbf{A}) = u - a,\ u,\ u + a$; $\lambda(\mathbf{A}_e) = u - a_e,\ u,\ u + a_e$, where ${a_e}^2 = p(p_e/\rho + 1)/\rho = a^2 - (p_\rho - p/\rho)$; and $\lambda(\mathbf{A}_\rho) = 0,\ 0,\ 0$. Thus the matrices $\mathbf{A}$ and $\mathbf{A}_e$ have a complete set of eigenvectors, but $\mathbf{A}_\rho$ does not. We note that $a_e = a$ and $\mathbf{A}_e = \mathbf{A}$ for a gas in which p depends linearly on ρ, viz. a thermally perfect gas. Furthermore we find

$$\mathbf{F} = \mathbf{F}_h + \mathbf{F}', \tag{3.3}$$

where $\mathbf{F}_h = \mathbf{A}\mathbf{U}$, and $\mathbf{F}' = \mathbf{A}_\rho\mathbf{U}$. That is, the flux vector $\mathbf{F}$ no longer posseses the property of homogeneity, rather is a sum of homogeneous and inhomogeneous parts. Since the matrix $\mathbf{A}$ has a complete set of eigenvectors, it can be readily diagonalized by a similarity matrix $\mathbf{S}$ whose column vectors are the right eigenvectors of $\mathbf{A}$:

$$\mathbf{A} = \mathbf{S}\Lambda\mathbf{S}^{-1}, \qquad \text{diag}\Lambda = \lambda(\mathbf{A}). \tag{3.4}$$

§3.1 Steger-Warming Splitting

By splitting the eigenvalues, $\Lambda = \Lambda^+ + \Lambda^-$, the real-gas version of Steger-Warming flux-vector splitting is obtained with $\mathbf{F}_h = \mathbf{F}_h^+ + \mathbf{F}_h^-$. The split fluxes are suited for upwind differencing. Note that, unlike in [8], the true speed of sound a of the gas is used to determine the switching between $\mathbf{F}_h^+$ and $\mathbf{F}_h^-$. Since $\mathbf{A}_\rho$ does not have a complete set of eigenvectors, an equation that includes $\mathbf{F}'$ alone does not have a hyperbolic charater. In consequence, central differencing, corresponding to the pseudo splitting

$$\mathbf{F}^\pm = {\mathbf{F}^\pm}_h + \frac{1}{2}\mathbf{F}', \tag{3.5}$$

may be appropriate. This has been verified in the numerical experiments of Section 4.

One cause of inaccuracy in the Steger-Warming splitting is that the split-flux derivatives are discontinuous when any of the eigenvalues $\lambda(\mathbf{A})$ changes sign. This gives rise to "glitches" in numerical solution, unless some extra smoothing is built into the flux formula. To solve this problem radically, Van Leer [3] developed a continuously differentiable splitting.

§3.2 Van Leer Splitting

In this section we present a most general and compact derivation of the Van Leer splitting that includes a family of flux choices and is easily applicable to curvilinear coordinates. It further is independent of the EOS used, and does not require homogeneity of the flux vector. Splitting takes place only when there exist eigenvalues of mixed signs, i.e.,

as $M^2 < 1$ for the system (3.1); M is the local Mach number based on a defined in (2.3). Since $u = Ma$, the mass flux $\mathbf{F}_1 = \rho a M$ is split as:

$$\begin{aligned} F_1 &= F_1^+ + F_1^-, \\ F_1^\pm &= \pm\frac{1}{4}\rho a(M \pm 1)^2. \end{aligned} \tag{3.6}$$

Note that the split fluxes $F_1^\pm$ have vanishing slope as $M \to \mp 1$, yielding smooth switching. This forms the basis for splitting of the remaining fluxes, namely, for expressing F_2 and F_3 in terms of $F_1^\pm$. Let us write

$$F_2 = (\rho u a)M + p, \tag{3.7}$$

where the first term on the RHS, representing the convection of momentum, already has the desired factor, $M = [(M+1)^2 - (M-1)^2]/4$. Now we must see if p can be written in terms of $(M+1)^2$ and $(M-1)^2$. Let us try the combination,

$$\begin{aligned} p &= x[(M+1)^2 - (M-1)^2] + y[(M+1)^2 + (M-1)^2] \\ &= 4xM + 2y(M^2+1). \end{aligned}$$

This leaves us one equation for two unknowns x and y. By choosing

$$2y = p,$$

which must be true anyway for $M = 0$, we find

$$x = -\frac{1}{4}pM$$

for arbitrary M. Thus p is recast as

$$p = \frac{p}{\rho a^2}[F_1^+(-u+2a) + F_1^-(-u-2a)]. \tag{3.8}$$

Substitution in (3.7) yields the splitting of $F_2 = F_2^+ + F_2^-$,

$$\begin{aligned} F_2^\pm &= F_1^\pm[u - \frac{p}{\rho a^2}(u \mp 2a)] \\ &= F_1^\pm[u - (u \mp 2a)/\Gamma]. \end{aligned} \tag{3.9}$$

We note that the last equality is obtained by the use of definition (2.6*b*) and is identical to the formula for an ideal gas.

We turn now to the splitting of the energy flux F_3. Again the flux contains a convection term:

$$F_3 = (\rho a E)M + pu,$$

where the factor M again can be represented as in F_2. Since p has factors $(u \pm 2a)$, it is natural to assume a quadratic function in u for pu; for symmetry reason this must have the form,

$$\begin{aligned} pu &= F_1^+(lu^2 + 2mua + na^2) + F_1^-(lu^2 - 2mua + na^2) \\ &= (l+m)\rho u^3 + (m+n)\rho u a^2. \end{aligned} \tag{3.10}$$

This leaves us many possibilities. We choose to eliminate ρu^3 by letting

$$l + m = 0,$$

hence

$$m + n = \frac{p}{\rho a^2}.$$

Consequently, a family of ∞ choices, with single parameter m, results for $F_3 = F_3^+ + F_3^-$,

$$F_3^\pm = F_1^\pm[H - m(u \mp a)^2], \tag{3.11}$$

The identical result is obtained when letting $(m+n)$ vanish, instead of $(l+m)$, because of the symmetric occurrence of u^2 and a^2. Van Leer's splitting is a member of this family, found by requiring that the terms in the square bracket form a perfect square. This leads to

$$m = \frac{\frac{h}{a^2}}{1 + 2\frac{h}{a^2}} \tag{3.12a}$$

and

$$F_3^\pm = \frac{1}{2}F_1^\pm\frac{(ua \pm 2h)^2}{(a^2+2h)}. \tag{3.12b}$$

For an ideal gas, this results in the nice property that one eigenvalue of each split-flux Jacobian vanishes, because $F_3^\pm$ depends solely on $F_1^\pm$ and $F_2^\pm$:

$$F_3^\pm = \text{const}\frac{(F_2^\pm)^2}{F_1^\pm}. \tag{3.12c}$$

As a result, numerical diffusion is minimal [12] and sharp steady shocks can be obtained. This property, however, is lost for the real gas. The particular eigenvalues still are very close to zero and may be either positive or negative. In the former case the formula has slightly increased dissipation, in the latter case it may actually make upwind differencing unstable. Neither effect is noticeable in practice; see numerical tests in Section 4. Another obvious choice is

$$\begin{aligned} m &= 0, \\ F_3^\pm &= F_1^\pm H. \end{aligned} \tag{3.13}$$

This has the advantage of being the simplest and most efficient formula possible; the ideal-gas version has one eigenvalue close to zero and positive. It was derived independently by Hänel et al [13].

When extending the split fluxes (3.9) and (3.11) to curvilinear multidimensional moving coordinates, we benefit from the fact that p and pu have been expressed in terms of $F_1^\pm$. The derivation is straightforward and yields the following formulas for the split fluxes in the direction of a coordinate ξ:

$$\begin{aligned} F_1^\pm &= \pm\frac{1}{4}\frac{\rho}{a}(\tilde{u} \pm a)^2 = \pm\frac{1}{4}\rho a(\tilde{M} \pm 1)^2, \\ F_2^\pm &= F_1^\pm[u - \xi_x(\tilde{u} \mp 2a)/\Gamma], \\ F_3^\pm &= F_1^\pm[v - \xi_y(\tilde{u} \mp 2a)/\Gamma], \\ F_4^\pm &= F_1^\pm[w - \xi_z(\tilde{u} \mp 2a)/\Gamma], \\ F_5^\pm &= F_1^\pm[H + \xi_t(\tilde{u} \mp 2a)/\Gamma - m(\tilde{u} \mp 2a)^2]. \end{aligned} \tag{3.15}$$

Here u, v and w are the Cartesian velocity components and $\tilde{u}$ is the contravariant ξ-velocity, i.e. the velocity normal to a moving surface of constant ξ; $\tilde{M}$ is the corresponding contravariant Mach number. The form is the same as for the ideal gas except the Γ, instead of γ, is used (see Thomas, Van Leer and Walters [14]).

Note that none of the differentiable splittings derived above involves special derivatives of the EOS. The only thermodynamic quantities needed are p and a, which are standard. Unlike in [8], no assumption of homogeneity of the flux $\mathbf{F}$ is required.

§3.3 Roe Splitting

To construct Roe's flux-difference splitting, one usually defines an average state $\hat{\mathbf{U}}$ such that

$$\triangle \mathbf{F} = \hat{\mathbf{A}} \triangle \mathbf{U}, \tag{3.16}$$

where $\triangle(\bullet) = (\bullet)_R - (\bullet)_L$, and the matrix $\hat{\mathbf{A}}(\mathbf{U}) = \frac{\partial \mathbf{F}}{\partial \mathbf{U}}$ has precisely the same form as in (3.2a)-(3.2c), but is evaluated at a particular average state, $\hat{\mathbf{U}} = \hat{\mathbf{U}}(\mathbf{U}_L, \mathbf{U}_R)$. Note that the difference between states "L" and "R" is not necessarily small.

The object now is to find an average state such that (3.16) is satisfied exactly for all admissible pairs $(\mathbf{U}_L, \mathbf{U}_R)$. In the ideal-gas case this is easily accomplished since (3.16) represents three relatively simple equations with three unknowns, the components of $\hat{\mathbf{U}}$. (Note, for instance, that the term $(p_\rho - p_e e/\rho)$ appearing in the first column of $\mathbf{A}$ vanishes.) In fact, the matrix $\mathbf{A}(\hat{\mathbf{U}})$ is completely determined by only two average state quantities as the density does not occur explicitly. The average Jacobian depends only on the quantities $\hat{u}$ and $\hat{H}$; an average density $\hat{\rho}$ may be chosen freely, although there is an obvious choice for it (see (3.19c)).

For a real gas, the simplicity is lost. The nonlinear system (3.16) must be solved numerically and in general may have more than one solution or no solution at all. In order to find a practical formula for $\hat{\mathbf{A}}$ we must allow independent averages of more than three state quantities to enter the elements of $\hat{\mathbf{A}}$. Judging from the form of $\mathbf{A}$ we have six non-constant elements to play with, so there is a room for six independent averages. We shall choose the set $(\hat{u}, \hat{\rho}, \hat{e}, \hat{H}, \hat{p_e}, \hat{p_\rho})$. We note that, the relation of the total enthalpy to the other flow quantities, i.e. $H = e + p/\rho + u^2/2$ while holding *pointwise*, does not necessarily hold for the average state quantities which are functions of two states.

The mass-flux equation in (3.16) is automatically satisfied for any average state. To satisfy the momentum-flux equation, we choose

$$\text{(i)} \qquad \triangle \rho u = \hat{\rho} \triangle u + \hat{u} \triangle \rho; \tag{3.18a}$$

$$\text{(ii)} \qquad \triangle \rho u^2 = 2\hat{\rho}\hat{u} \triangle u + \hat{u}^2 \triangle \rho. \tag{3.18b}$$

Let the Roe-average operator μ be defined as:

$$\mu(f) = \frac{r_R f_R + r_L f_L}{r_R + r_L}, \qquad r = \rho^{\frac{1}{2}}. \tag{3.19a}$$

The conditions (i) and (ii) are met by

$$\hat{u} = \mu(u), \tag{3.19b}$$

$$\hat{\rho} = r_L r_R. \tag{3.19c}$$

Assuming further that,

$$\text{(iii)} \qquad \triangle \rho e = \hat{\rho} \triangle e + \hat{e} \triangle \rho, \tag{3.20a}$$

which is met by

$$\hat{e} = \mu(e), \tag{3.20b}$$

the second equation of (3.16) is then satisfied by

$$\text{(iv)} \qquad \triangle p = \hat{p_e} \triangle e + \hat{p_\rho} \triangle \rho. \tag{3.21}$$

Finally, we find that the energy-flux equation is readily satisfied by setting

$$\text{(v)} \qquad \triangle \rho u H = \hat{\rho} \hat{H} \triangle u + \hat{u} \triangle \rho H, \tag{3.22a}$$

hence

$$\hat{H} = \mu(H). \tag{3.22b}$$

Left to be completed are the definitions of $\hat{p_e}$ and $\hat{p_\rho}$. Glaister [10] suggests

$$\begin{aligned} \hat{p_e} &= \frac{p_E - p_W}{\triangle e}, \\ \hat{p_\rho} &= \frac{p_S - p_N}{\triangle \rho}. \end{aligned} \tag{3.23a}$$

where p_E, p_W, p_S, and p_N are approximated at points shown in the sketch by algebraic averaging

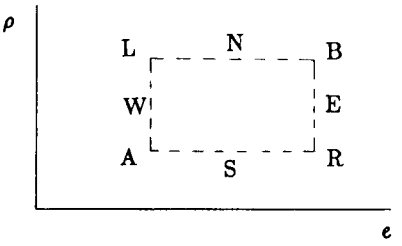

i.e.,

$$\begin{aligned} p_E &= \frac{1}{2}(p_R + p_B), \qquad & p_B &= p(\rho_L, e_R), \\ p_W &= \frac{1}{2}(p_L + p_A), \qquad & p_A &= p(\rho_R, e_L), \\ p_N &= \frac{1}{2}(p_L + p_B), \\ p_S &= \frac{1}{2}(p_R + p_A). \end{aligned} \tag{3.23b}$$

With this choice, (3.21) is met precisely. However, the artificially introduced states, A and B, cause problems at discontinuities, in particular for a contact discontinuity across which the density and internal energy jump appreciably. If the EOS is a non-convex function(as for an ideal gas) and L and R are two admissible discrete states, then A and B can lie outside the region of validity of the EOS. This will manifest itself in a calculation in the form of oscillations near the discontinuity, and/or an inaccurate solution.

This leads to

$$\hat{p_e} = \frac{1}{2}[(\triangle p - \bar{p_\rho}\triangle\rho)/\triangle e + \bar{p_e}],$$
$$\hat{p_\rho} = \frac{1}{2}[(\triangle p - \bar{p_e}\triangle e)/\triangle\rho + \bar{p_\rho}]. \tag{3.24}$$

It is easily verified that, of all the pairs $(\hat{p_\rho}, \hat{p_e})$ satisfying (3.21), the pair (3.24) lies closest to $(\bar{p_\rho}, \bar{p_e})$ and must be considered the optimal choice regarding consistency. The formulas suggested by Vinokur and Liu [9] are based on a different choice of independently averaged quantities, with different constraints, and are more complicated.

4. NUMERICAL TEST

Extensive tests over a wide range of flow conditions have been conducted to validate the accuracy of the present formulation. Some extreme cases of 1D unsteady shock tube and steady nozzle problems are presented in this paper; the performance of these split fluxes are compared against the exact solution. The result of accounting for real-gas effect is discussed.

The Euler equations are integrated using the explicit Lax-Wendroff scheme. To obtain a crisp and monotone shock representation, the TVD scheme based on the above split formulas, as described in [11], is employed, along with the super-Bee limiter [15] for steepening of the contact discontinuity.

The computation domain consists of 200 and 100 equally-spaced intervals for the shock-tube and nozzle problems, respectively.

§4.1 Shock-Tube Problem

The initial conditions are those used in [8]:
For $0 \leq x \leq 5$,

$$p_4 = 100 \text{ atm},$$
$$T_4 = 9000 \text{ K},$$
$$u_4 = 0;$$

And $5 \leq x \leq 10$,

$$p_1 = 1 \text{ atm},$$
$$T_1 = 300 \text{ K},$$
$$u_1 = 0.$$

The EOS is generated using the widely referred program by Gordon and McBride [16] for equilibrium air in the range 250 K $\leq T \leq$ 12000 K, 0.1 atm $\leq p \leq$ 100 atm, in which 17 species are included. With over 3600 sets of state points, a least-square fit for pressure is obtained with 20 basis functions of (ρ, e). The resulting standard deviation does not exceed 0.2%, the maximum value occurs, as expected, on the boundary.

The procedure for finding the "exact" solution basically is similar to that of [7] except for differences in the details of the numerical steps. We iterate the system via Newton's procedure; the pressure behind the shock p_2 is iterated until the velocity integrated through the rarafaction fan and the velocity obtained from the jump relation across the shock are equal at the contact discontinuity. The procedure converges in only a few iterations.

Figures 1-3 show the numerical results of the Roe, Van Leer and Steger-Warming splittings for, respectively, $\rho/\rho_4, u/u_4, p/p_4$ and e/e_4, together with exact solutions for real and ideal gases. The jump across the contact is rather large, about one order of magnitude. This is a difficult case to calculate, as the initial temperatures differ by a factor 30 and consequently the compositions of the air are completely different. It has been our experience that the TVD scheme can handle large differences in pressure very well, but not as well if there also are large temperature differences. Nevertheless, our numerical results generally show excellent agreement with the exact solution. A crisp shock profile is seen, while the effect of dissipation at the contact discontinuity remains as in the case of the ideal gas, but accompanied by slight oscillations. Among all three splittings, the Roe scheme seems to give the best results, especially near the contact discontinuity.

The species molar fractions obtained by the Roe splitting are shown in Fig. 4. The sharp peak in the NO molar fraction is a numerical result produced by the smearing of internal energy at the contact discontinuity. This is because the NO molar fraction is a very strong, non-monotone function of temperature (internal energy), and is most stable at some intermediate temperature across the "numerical" contact discontinuity. It is seen that a large amount of recovery of O_2 and N_2 from O and N occurs across the contact due to the large temperature drop, while there is only a minute change across the shock. This is also the case for electrons, N^+ and NO^-.

The results of excluding the real-gas effect are also displayed for air with the same initial pressure and temperature as well as at the same final t (=0.0015 sec). This amounts to taking $p = 0.4\rho e$ for the EOS. Significant dissociation and ionization take place at high temperatures in the real gas, thereby yielding a much larger specific internal energy and lower density than in the ideal gas. The shock and rarefaction wave in the ideal gas are travelling at a slower speed; the shock strength and the jump across the contact discontinuity also appear weaker.

Similar numerical results were obtained by Montagné, Yee and Vinokur [17], based on the split-flux formulas of [9]. The parameters of the shock-tube problems solved in [17] are different from those of Figures 1-4 and do not go beyond a temperature jump of a factor 10 at the contact surface. Disregarding this difference, the results appear to be of comparable accuracy.

§4.2 Steady Nozzle Problem

Calculations for steady real-gas flows in 1D convergent-divergent and divergent nozzles are given along with the exact ideal-gas solutions. The area distribution of the nozzle are listed below.
Convergent-divergent nozzle:

$$A(x) = 5.5 - 4.5\ cos(\frac{x-4}{6}\pi), \qquad 4 \leq x \leq 10;$$
$$A(x) = 1.2 - 0.2\ cos(\frac{x-4}{4}\pi), \qquad x \leq 4.$$

Divergent nozzle:

$$A(x) = 5.5 + 4.5\ tanh(0.7x - 3.5), \quad 0 \leq x \leq 10.$$

Figures 5-7 show the results $p/p_{t\infty}$, ρ/ρ_∞, u/a_∞, and e/e_∞ for the convergent-divergent nozzle. Excellent agreement is achieved by all three schemes with monotone and sharp resolution across the shock, although Steger-Warming's is slightly more dissipative and smears over about 2 interior cells. The kink at the throat resulting from the discontinuity of area curvature, $A''(x)$, is resolved well. The ideal-gas shock wave in this case is slightly further upstream and the jumps in velocity and energy become weaker. As in the shock-tube problem, the high inflow temperature produces significant dissociation and ionization. Consequently, the internal energy more than doubles that of the ideal gas. The molar fraction of N, O, electrons and NO^+ in Fig. 8 is decreased by the continued drop in temperature associated with the acceleration of the gas up until at the shock, but is increased abruptly by the shock. The molar fraction of N_2, O_2 and NO simply reverses the trend due to the conservation of mass.

Calculations are also carried out for flows in the divergent nozzle; the results are given in Figs. 9-12. The shock wave is stronger than the above case, but the flow variations are generally similar. In this particular set of area geometry and flow parameters, the real-gas and ideal-gas shock locations are essentially identical.

CONCLUDING REMARKS

Care in deriving flux-vector and flux-difference splittings for a real gas pays off, as evidenced by the quality of the numerical results presented above. This is gratifying, because most formulas derived above, viz. the extensions of Van Leer's differentiable flux-vector splitting and Roe's flux-difference splitting are close to being mathematically unique. The Steger-Warming splitting may be derived differently but we saw neither the way nor the need to do so.

From the numerical results for the shock-tube problem it is clear that the constraint on the width of a contact discontinuity is even more stringent for a real gas than for an ideal gas. The fictitious discrete states in a numerical profile representing a contact discontinuity trigger non-trivial chemistry, disturbing the pressure equilibrium that is so easily found for the ideal gas.

ACKNOWLEDGMENT

The authors would like to thank B. McBride of NASA Lewis Research Center for her kind help in generating equilibrium air data.

REFERENCES

1. S. K. Gudonov, 'A Finite-Difference Method for the Numerical Computation of Discontinuous Solutions of the Equations of Fluid Dynamics,' *Mat. Sb.* **47**, 271 (1959).
2. J. L. Steger and R. F. Warming, 'Flux vector splitting of the inviscid gasdynamics equations with application to finite difference methods,' *J. Comput. Phys.* **40**, 263 (1981).
3. B. van Leer, 'Flux-vector splitting for the Euler equations,' *Lecture Notes in Physics* **170**, 507 (1982).
4. P. L. Roe, 'Approximate Riemann solvers, parameter vectors, and difference schemes,' *J. Comput. Phys.* **43**, 357 (1981).
5. S. Osher, 'Numerical Solution of Singular Perturbation Problems and Hyperbolic Systems of Conservation Laws,' *North Holland Math. Studies* **47**, 179 (1981).
6. A. Harten, P. D. Lax and B. van Leer, 'Upstream Differencing and Gudonov-Type Schemes for Hyperbolic Conservation Laws,' *SIAM Rev.* **25**, 35 (1983).
7. P. Collela and H. M. Glaz, 'Efficient Solution Algorithms for the Riemann Problem for Real Gases,' *J. Comput. Phys.* **59**, 264 (1985).
8. B. Grossman and R. W. Walters, 'An Analysis of Flux-Split Algorithms for Euler's Equations with Real Gases,' AIAA paper 87-1117-CP, 1987 (unpublished).
9. M. Vinokur and Y. Liu, 'Equilibrium Gas Flow Computations II: An Analysis of Numerical Formulations of Conservation Laws,' AIAA paper 88-0127, 1988 (unpublished).
10. P. Glaister, 'An Approximate Linearised Riemann Solver for the Euler Equations for Real Gases,' *J. Comput. Phys.* **74**, 382 (1988).
11. M.-S. Liou, 'A Generalized Procedure for Constructing an Upwind-Based TVD Scheme,' AIAA paper 87-0355, 1987 (unpublished).
12. B. van Leer, J. L. Thomas, P. L. Roe and R. W. Newsome, 'A comparison of numerical flux formulas for the Euler and Navier-Stokes equations,' AIAA paper 87-1104-CP, 1987 (unpublished).
13. D. Hänel, R. Schwane and G. Seider, 'On the Accuracy of Upwind Schemes for the Solution of the Navier-Stokes Equations,' AIAA paper 87-1105-CP, 1987 (unpublished).
14. J. L. Thomas, B. van Leer and R. W. Walters, 'Implicit Flux-Split Schemes for the Euler Equations,' AIAA paper 85-1680, 1985 (unpublished).
15. P. L. Roe, 'Characteristic-Based Schemes for the Euler Equations,' *Ann. Rev. Fluid Mech.* **18**, 337 (1986).
16. S. Gordon and B. J. McBride, 'Computer Program for Calculation of Complex Chemical Equilibrium Compositions, Rocket Performance, Incident and Reflected Shocks, and Chapman-Jouguet Detonations,' NASA SP-273, 1976 (unpublished).
17. J.-L. Montagné, H.C. Yee and M. Vinokur, 'Comparative Study of High-Resolution Shock-Capturing Schemes for a Real Gas,' NASA TM 100004, 1987 (unpublished).

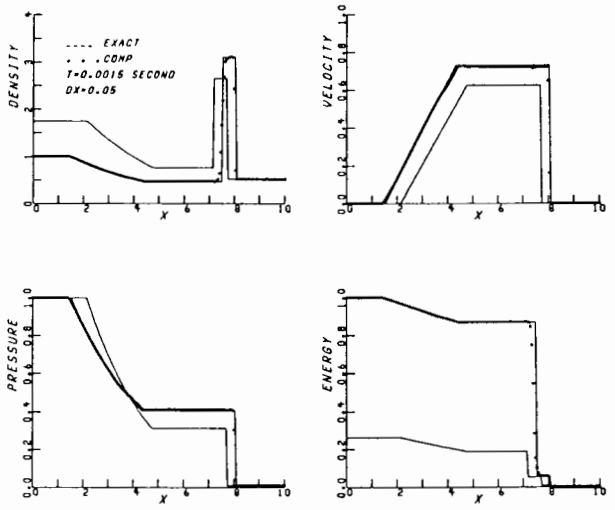

Figure 1. Shock tube problem, Roe flux-difference splitting.

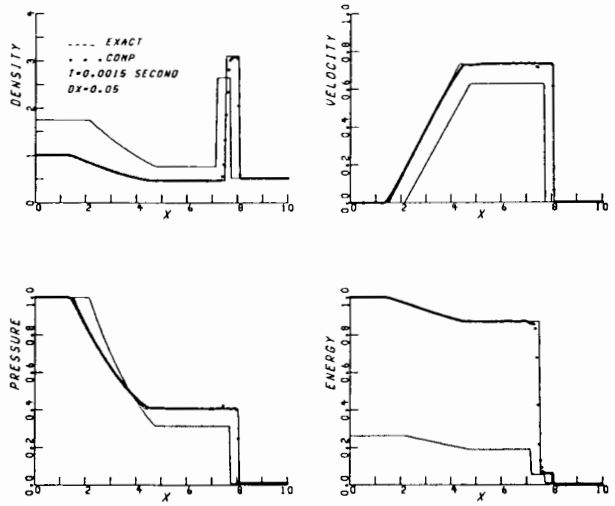

Figure 2. Shock tube problem, Steger-Warming flux-vector splitting.

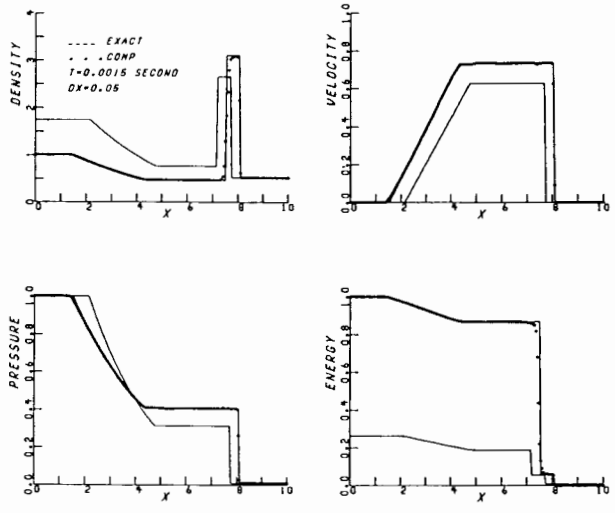

Figure 3. Shock tube problem, Van Leer flux-vector splitting.

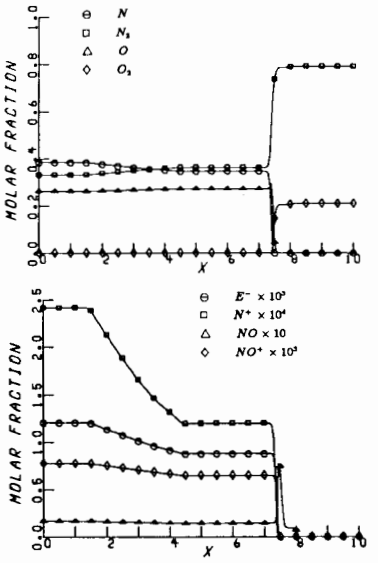

Figure 4. Shock tube problem, molar fractions of species.

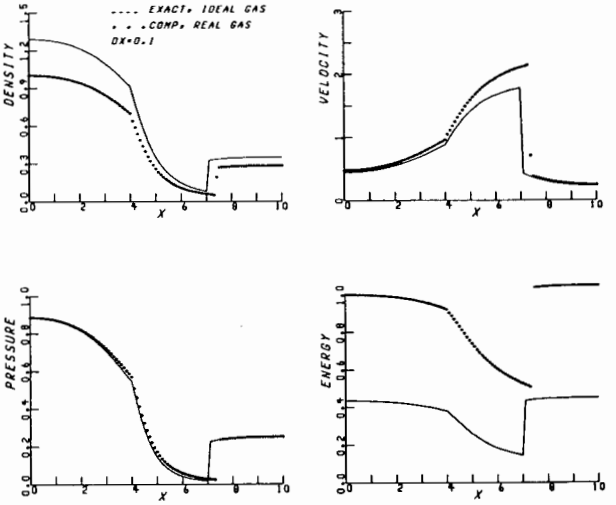

Figure 5. Convergent-divergent nozzle problem, Roe flux-difference splitting.

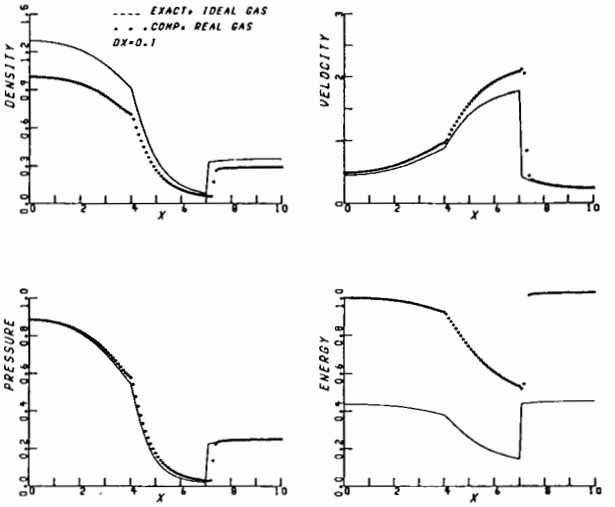

Figure 6. Convergent-divergent nozzle problem, Steger-Warming flux-vector splitting.

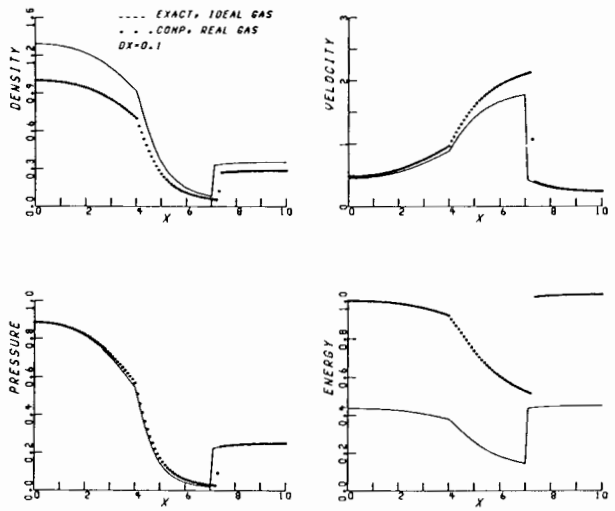

Figure 7. Convergent-divergent nozzle problem, Van Leer flux-vector splitting.

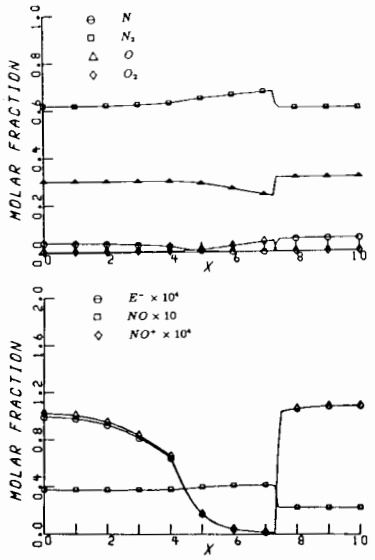

Figure 8. Convergent-divergent nozzle problem, molar fractions of species. Roe splitting.

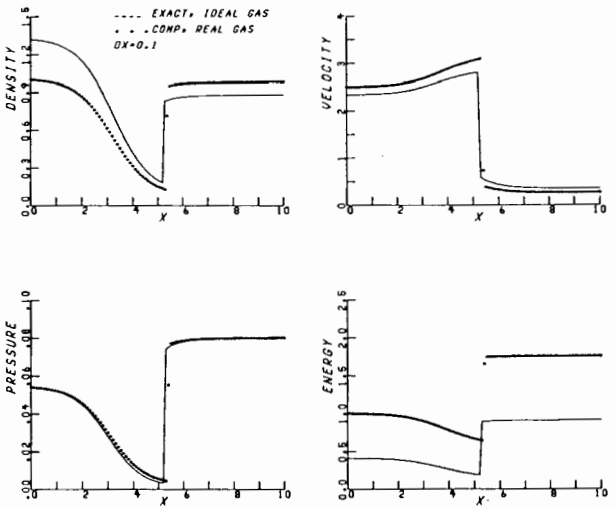

Figure 9. Divergent nozzle problem, Roe flux-difference splitting.

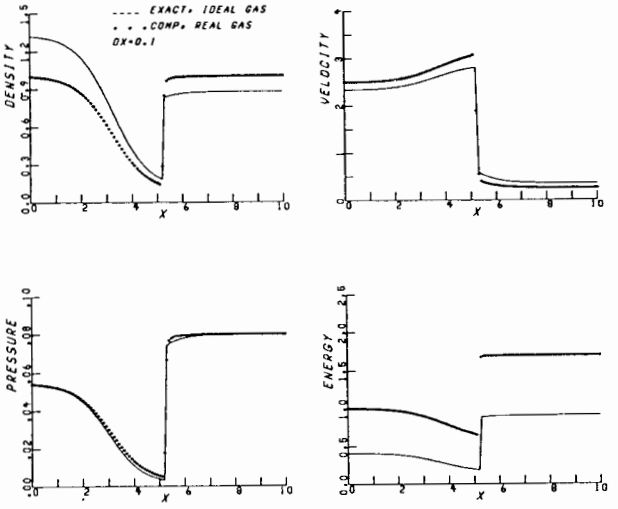

Figure 10. Divergent nozzle problem, Steger-Warming flux-vector splitting.

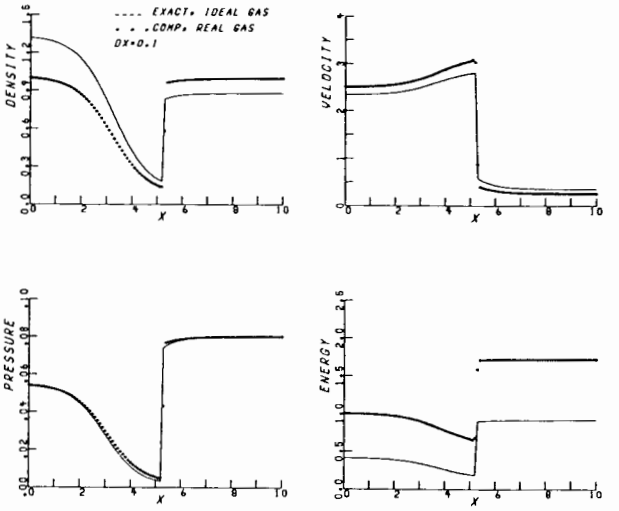

Figure 11. Divergent nozzle problem, Van Leer flux-vector splitting.

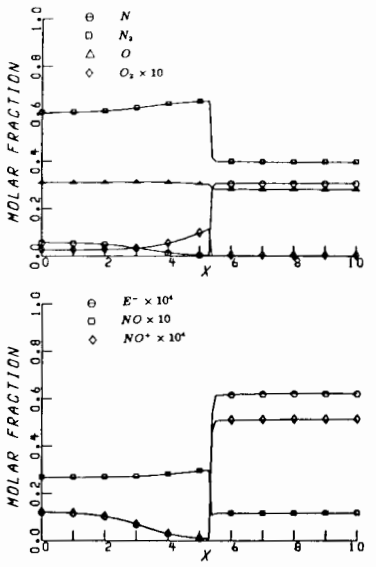

Figure 12. Divergent nozzle problem, molar fractions of species. Roe splitting.